water

MDPI

Article

Application of the Entropy Model to Estimate Flow Discharge and Bed Load Transport with Limited Field Measurements

Farhad Bahmanpouri [1,*], Anshul Yadav [2], Christian Massari [1], Domenico De Santis [3], Ashutosh Sharma [2], Ankit Agarwal [2], Sumit Sen [2], Luigi Fraccarollo [4], Tommaso Moramarco [1] and Silvia Barbetta [1]

[1] Research Institute for Geo-Hydrological Protection, National Research Council (CNR), 06128 Perugia, Italy; christian.massari@irpi.cnr.it (C.M.); t.moramarco@irpi.cnr.it (T.M.); silvia.barbetta@cnr.it (S.B.)
[2] Department of Hydrology, IIT Roorkee, Roorkee 247667, India; ayadav@hy.iitr.ac.in (A.Y.); ashutosh.sharma@hy.iitr.ac.in (A.S.); ankit.agarwal@hy.iitr.ac.in (A.A.); sumit.sen@hy.iitr.ac.in (S.S.)
[3] Research Institute for Geo-Hydrological Protection, National Research Council, 87036 Rende, Italy; domenico.desantis@cnr.it
[4] Department of Civil, Environmental and Mechanical Engineering, University of Trento, 38123 Trento, Italy; luigi.fraccarollo@unitn.it
* Correspondence: farhadbahmanpouri@cnr.it

Abstract: Sediment transport can be observed within the flow of water in rivers, canals, and coastal regions, encompassing both suspended-load transport and bed-load transport. Bed-load transport specifically occurs near the riverbed, playing a crucial role in the formation of the riverbed itself. The current study aimed to explore the process of sediment transport by employing the entropy concept as a theoretical approach. To this end, field data collected using a current meter in the Alaknanda River at Srinagar in India were utilized. A comparison was made between the calculated mean velocity and discharge values and the observed data obtained from the Central Water Commission (CWC), demonstrating a maximum error percentage of 9%. Subsequently, shear velocity was determined for various cross-sections under different flow scenarios. The Shields parameter was then derived from the shear-velocity distribution to evaluate the transport potential of the sediment particles. The model results showed varying bed-load transport rates that increased as the particle size decreased and the discharge rate increased. In conclusion, the study findings highlight the efficacy of utilizing the entropy theory for estimating flow discharge and sediment transport in developing countries.

Keywords: entropy model; velocity distribution; sediment transport; developing countries; current meter

check for updates

Citation: Bahmanpouri, F.; Yadav, A.; Massari, C.; De Santis, D.; Sharma, A.; Agarwal, A.; Sen, S.; Fraccarollo, L.; Moramarco, T.; Barbetta, S. Application of the Entropy Model to Estimate Flow Discharge and Bed Load Transport with Limited Field Measurements. *Water* **2024**, *16*, 3684. https://doi.org/10.3390/w16243684

Academic Editor: Jianguo Zhou

Received: 15 October 2024
Revised: 11 December 2024
Accepted: 14 December 2024
Published: 20 December 2024

Copyright: © 2024 by the authors. Licensee MDPI, Basel, Switzerland. This article is an open access article distributed under the terms and conditions of the Creative Commons Attribution (CC BY) license (https://creativecommons.org/licenses/by/4.0/).

1. Introduction

Bed-load transport, induced by the movement of particles as they roll, slide, or advance through a series of small jumps known as saltation along a stream bed, is of particular importance in shaping river morphology. Although suspended loads generally dominate in the annual sediment deposition volume in natural rivers, bed-load transport results in significant morphological changes [1]. The process of bed-load transport controls various aspects of morphological changes in river systems. This includes bank erosion, bed forms, and the pace at which the river cuts into the surrounding relief [2]. Many researchers have indicated that the driving force of sediment transport can be expressed in terms of boundary shear stress [3–12].

Various formulas have been developed to estimate bed-load transport in rivers with different particle diameters, ranging from simple regressions to complex multiparameter formulations. Researchers have applied these relationships to investigate bed-load transport in natural rivers [13–15] and in laboratory experiments [16–18].

One of the most promising approaches for leveraging river velocity and discharge is based on the concept of entropy. Researchers have extensively utilized this method to

forecast velocity patterns and various significant parameters within open channels [19–27]. Termini and Moramarco [28] determined the cross-sectional velocity through the application of the entropy concept and the examination of the spatial distribution of the entropic parameter, M, in conjunction with the placement of the velocity dip. Abdolvandi et al. [29] formulated a novel procedure for estimating the conversion factor, defined as the ratio between the mean velocity and the maximum one, by utilizing a one-dimensional flood routing model and an entropy velocity profile. Their method involved the estimation of discharge at poorly gauged sites based on the assumption that the constant velocity factor depends both on the ratio between maximum and mean velocities and on the aspect ratio (i.e., the ratio of the river width to depth). Chahrour et al. [30] applied a picture-based methodology to quantify the discharge of the Isère River at Grenoble University Campus, employing an entropy-based approach. Furthermore, the utilization of a particle-tracking velocimetry (PTV) approach has enabled the estimation of surface velocities from video imagery, which can be subsequently utilized for entropy calculations. Vyas et al. [31] analyzed the entropy concept using point velocity data obtained at a depth of $0.6D$ from the water surface, where D represents the total water depth. They established a correlation between the maximum point velocity derived from the sectional mean flow velocity and the maximum point velocity estimated at a depth of $0.6D$. Bahmanpouri et al. [32] utilized ADCP surface-velocity measurements from various cross-sections to apply the entropy methodology at the confluence of the Negro and Solimões rivers. Despite the intricate hydrodynamic conditions, their study effectively predicted the velocity field and flow discharge utilizing the entropy method. Ammari et al. [33] implemented the entropy concept to calculate the discharge rate by utilizing single-parameter estimation for the drainage network in a vast region encompassing the central and eastern parts of Algeria. Their findings indicated a uniform spatial distribution of the entropy parameter along the channels, enabling discharge estimation using only a few measurements of the maximum velocity and water surface level. Bahmanpouri et al. [34] estimated the cross-sectional velocity and discharge along two European rivers based on a single surface-velocity measurement provided by an unmanned aerial vehicle (UAV), achieving errors below 13%. Recently, Ahamed and Kundu [35] and Patel and Sarkar [36] used the entropy theory to estimate suspended sediment transport in rivers. They compared the computed values with experimental data on sediment discharge and found good agreement. Bahmanpouri et al. [37] applied the entropy model and the CFD three-dimensional simulations to investigate the bridge pier effect on the river flow.

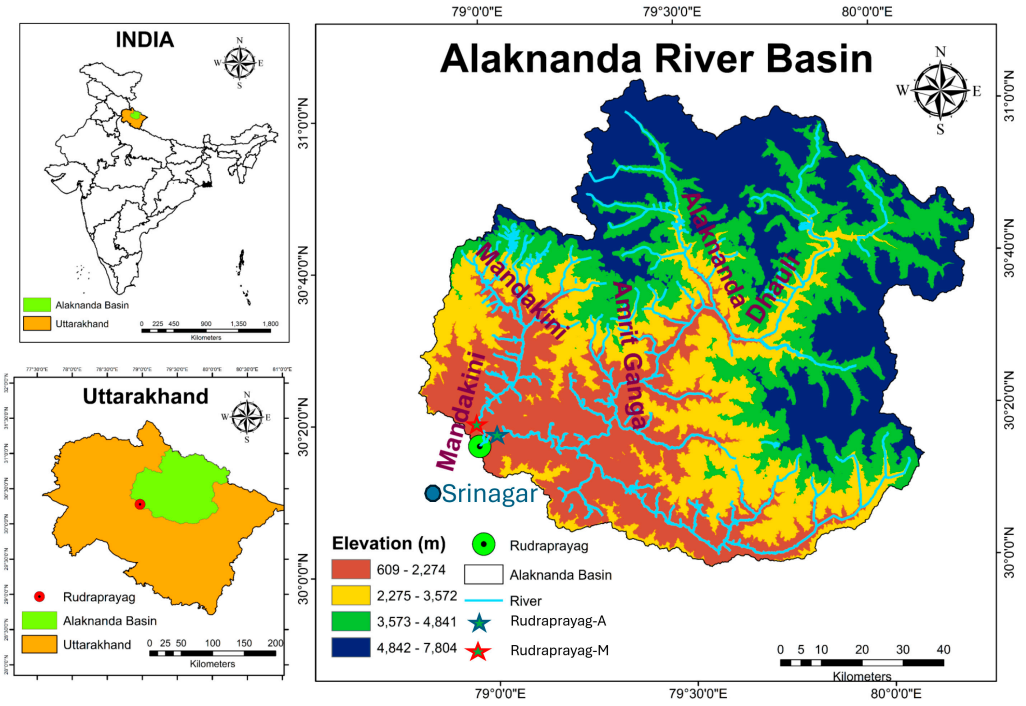
Building upon the previous applications of the entropy theory in investigating river flow dynamics, the current study aimed to extend the entropy theory to estimate cross-sectional velocity distributions, flow discharge, shear stress, and bed-load transport under different flow conditions. The study focused on developing countries, where field velocity measurements are often limited due to the lack of available devices and technology, especially during high flow conditions.

2. Materials and Methods

2.1. Study Area

The study area is in the northwest part of the Himalayan state of Uttarakhand. The length of the river stretch is approximately 100 km (Figure 1). The total catchment area of the Alaknanda River is 10.57×10^3 km^2. Numerous cloudburst-induced flash floods, landslides, and related erosion were reported in the Alaknanda River Basin, Uttarakhand [38]. Based on the data from 1990 to 2020, Table 1 shows the return period of the floods. The grain size distribution (GSD) of the bed particles is provided in Figure 1c. The bulk sediment samples, collected from a 1 m $\times$ 1 m pit and weighing approximately 136 kg, were used to assess the grain size distribution (GSD) of the streambed using the criteria suggested by Church [39] and following the methods of previous studies [40]. Sieve analysis of the dried sediment samples, using sieves ranging from 2 mm to 256 mm, revealed D_{50} and D_{84} (the grain size

at which 50% and 84% of the sediment sample, by weight, are finer, respectively) values of 72 mm and 170 mm, respectively.

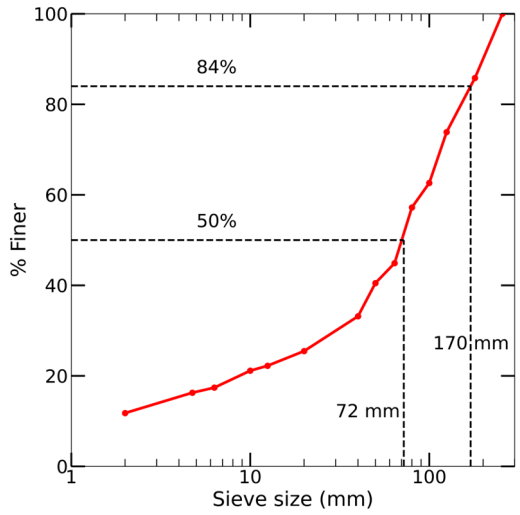


(**a**)



(**b**)

Figure 1. *Cont.*



(**c**)

Figure 1. Study area. (**a**) Alaknanda River Basin map illustrating its elevation ranges; (**b**) aerial photography from study area showing low flow condition and discharge of 355.4 m^3/s (horizontal scale); (**c**) grain size distribution (GSD) of bed particles.

Table 1. Flood return periods based on 1990–2020 data.

Flow Condition	Discharge (m^3/s)	Return Period
Low flow	355	<1 year
Moderate flow	948	<1 year
High flow	1587.9	<1 year
Flood in 2013	13,900	>1000 years
	4500	50 years
	4800	100 years
	5000	200 years
	5500	500 years

The return period was estimated through a statistical analysis of the time series of the maximum annual discharge for the period of 1990–2020, reconstructed at the site of Srinagar by considering the observed daily values at Rudraprayad-A and Rudraprayad-B, which are located upstream of a confluence (Figure 1a). Specifically, the observed flow at Srinagar was assessed by adding the two upstream discharges. The observed data at Srinagar are available for the period of 2019–2020 and they were used for validation of the reconstructed discharge series at Srinagar by adding the upstream discharges. The fitted lognormal probability distribution allowed us to quantify the return period for the considered streamflow values. The low-, medium-, and high-flow conditions were identified in the actual daily time series of the investigated sites (daily discharge in 2019–2020). Specifically, on average, low flow refers to baseflow or slightly greater, medium flow refers to half-bankfull flow, and high flow refers to close to bankfull flow. All of these conditions were characterized by low return periods because the reconstructed discharge values for 1990–2020 were mostly higher.

2.2. Entropy Theory

The entropy theory is based on a physical system that may have many states, *Xj*, each with an assigned probability, *P*(*Xj*). When the physical system has assigned constraints, the entropy tends towards a maximum value as random states tend to occur in conditions with

the greatest possible disorder. At each stage, an information content, $I(Xj)$, is associated with $I(Xj) = -\ln P(Xj)$ and the entropy value, $H(X)$, for a continuous state variable X, which represents the mean of $I(X)$ (Janes, 1957a, b), i.e., $H(X) = -\int P(X) lnP(X) dX$, with $p(X)$ representing the probability density function. In other words, if $X = Xj$ is a certain event, its entropy goes to zero, while if $P(Xj)$ tends toward 0, the information content, i.e.,$-lnP(Xj)$, tends toward ∞. Therefore, entropy is used for statistical inference to solve a probability distribution function when the information about the variable is limited to some average quantities, which are defined as constraints such as mean and variance. In the application of entropy to streamflow measurements, the pioneer was Chiu [41], who identified the probability distribution of velocity in the cross-sectional flow area by maximizing the entropy of the flow state. Chiu [41] developed a probabilistic formulation that introduced the concept of velocity distribution in the probability domain. This was implemented by considering the random sampling of flow velocity data in a channel section. However, it could be challenging to obtain such data. In this direction, Chiu proposed a link between the probability and physical domains. He derived possible expressions of the cumulative probability distribution function according to the coordinates in the physical space. The probability density function of the velocity was achieved by applying the maximum entropy principle [20,41,42]. Using the probabilistic formulation, the mean velocity could be expressed as a linear function of the maximum velocity through the dimensionless entropic parameter M [43]. The M value is a fundamental measure of information about the characteristics of the channel section, such as changes in the bed form, slope, and geometric shape [44]. In this context, M is a dimensionless entropic parameter that describes the variability or randomness of the velocity distribution in the flow. It reflects the degree of uniformity in the velocity profile, where larger values of M correspond to more uniform distributions. The function $\phi(M)$ represents the dimensionless velocity ratio, defined as the ratio of the mean velocity to the maximum velocity. This relationship is expressed in the equation provided. The parameter $\phi(M)$ is obtained by integrating the two-dimensional velocity distribution in the cross-sectional flow area [42] and captures how the mean velocity is distributed relative to the maximum velocity. Moramarco and Singh [24] showed that $\phi(M)$ does not rely on the dynamic of flow, represented by the energy slope S_f, only on hydraulic parameters such as roughness and hydraulic radius. In the case of flow where secondary currents are significant, $\phi(M)$ is expected to have low values, and this entails velocity profiles showing a clear curvature with a high dip (location of the maximum velocity below the water surface). It was noted that the limitation of this model in developing countries is that it cannot be applied in areas where surface-velocity measurements are not feasible.

Mean velocity data for a channel cross-section are particularly important for hydraulic applications. To estimate discharge, it is essential to efficiently determine the mean velocity. The mean cross-sectional flow velocity can be reliably calculated using the ratio between the mean and maximum velocities of a specific cross-section that approaches a constant value. In this direction, Chiu [20] formulated a computation method for assessing cross-sectional velocity distribution, $U(x,y)$, employing the entropy probability density function. Subsequently, Moramarco et al. [45] simplified the computation. Equation (1) is obtained using the Principle Of Maximum Entropy (POME), which states that an a posteriori probability distribution can be inferred by maximizing the entropy that is subject to constraints. In other words, for a given set of information, the best possible distribution that fits the data would be the one with the maximum entropy because this contains the most reliable assignment of probabilities. Therefore, Equation (1) represents the best possible velocity distribution obtained by maximizing the entropy, following the procedure proposed by Chiu [41,42]. By applying this methodology, it becomes feasible to ascertain the velocity profile based on entropy along the verticals:

$$U(x_i, y) = \frac{U_{maxv}(x_i)}{M} \ln\left[1 + \left(e^M - 1\right) \frac{y}{D(x_i) - h(x_i)} \exp\left(1 - \frac{y}{D(x_i) - h(x_i)}\right)\right] \quad i = 1 \ldots N_v \tag{1}$$

where U is the time-averaged velocity, $U_{maxv}(x_i)$ is the maximum value of U along the ith vertical, x_i is the distance of the ith sampled vertical from the left bank, $h(x_i)$ is the dip (i.e., the depth of $U_{maxv}(x_i)$ below the water surface), $D(x_i)$ is the flow depth, y is the distance of the velocity point from the bed, and N_v is the number of verticals sampled across the river section. For the gauged sites, the estimation of M can be conducted by utilizing the linear entropic relationship, which incorporates the mean and maximum flow velocities, namely U_m and U_{max}. These velocities are measured across the entire cross-section, as suggested by Chiu [20]:

$$\phi(M) = \frac{U_m}{U_{max}} = \left(\frac{e^M}{e^M - 1} - \frac{1}{M}\right) \tag{2}$$

U_m and U_{max} are collected for steady flow conditions, and in general, for a given river site, $\phi(M)$ remains constant for all flow conditions [45]. However, for ungauged sites where U_m or discharge data are unavailable, the entropic function $\phi(M)$ can be estimated using the method proposed by Moramarco and Singh [24]:

$$\phi(M) = \frac{\frac{1}{n}R^{\frac{1}{6}}}{\sqrt{g}\frac{1}{k}\left[\ln\left(\frac{y_{max}}{y_o}\right) + \frac{h}{y_{max}}\ln\left(\frac{h}{D}\right)\right]} = \left(\frac{e^M}{e^M - 1} - \frac{1}{M}\right) \tag{3}$$

where y_{max} is the location of U_{max} from the bottom, y_o is the datum where the velocity is equal to zero, k is the von Karman constant, R is the hydraulic radius, n is the Manning roughness, and D is the maximum flow depth. Suppose there are no data available to apply these two equations. In that case, we can use the trial-and-error method to estimate the optimal entropic parameter, M. By selecting an initial value for M, the entropy model will be implemented, and based on the velocity outputs U_m and U_{max}, $\phi(M)$ and M will be recalculated. This process will continue until the error is minimized [46]. For the current study, discharge data were obtained through measurements using a current meter.

At a river site where only the surface velocities, $U_{surf}(x_i, D(x_i))$, are available, then $U_{maxv}(x_i)$ can be estimated as follows [47]:

$$U_{maxv}(x_i) = \frac{U_{surf}(x_i, D(x_i))}{\frac{1}{M}\ln\left[1 + (e^M - 1)\delta(x_i)e^{1-\delta(x_i)}\right]} \tag{4}$$

where $\delta(x_i) = D(x_i)/[D(x_i) - h(x_i)]$. Specifically, if $h(x_i) = 0$, it follows that $\delta(x_i) = 1$ and hence, $U_{maxv}(x_i) = U_{surf}(x_i, D(x_i))$. The magnitude of $\delta(x_i)$ can be obtained based on the iterative procedure proposed by Termini and Moramarco [27]. This procedure can be applied for sites with a given $\phi(M)$. This procedure is based on assigning an initial dip, $h(x_{i,p=1})$, where the maximum surface velocity occurs (p is the iteration). For the current study, according to the initial value of the dip, a laboratory distribution law of dips suggested by Yang et al. [48] was implemented, and the $U_{maxv}(x_{i,p=1})$ as assessed using Equation (4) for all the considered verticals. $U_{max(p=1)}$ was identified as the maximum of $U_{maxv}(x_{i,p=1})$. Therefore, once $U_{maxv}(x_{i,p=1})$ is replaced in Equation (1), it allows for the calculation of the average velocities at each point along the velocity profile. It is worth mentioning that a constant velocity index, $\alpha = 0.85$, is commonly applied in the literature to relate the surface velocity to the depth-averaged velocity under the assumption of a monotonous velocity profile [49]. This index, however, is dependent on the vertical velocity profile characteristics [50], which are influenced by several factors, including the flow aspect ratio, micro- and macro-roughness, and the Froude and Reynolds numbers [51]. The potential presence of the dip phenomenon, induced by secondary currents, may challenge this assumption, resulting in non-monotonous velocity distributions. Consequently, the velocity index value may no longer accurately represent the two-dimensional spatial velocity distribution, leading to inaccuracies in discharge estimation. The entropic velocity distribution method that has been developed to overcome this issue can be effectively utilized. In the current study, the measured velocity from the current meter was converted to surface velocity based on the method developed by Vyas et al. [31]. For the first iteration,

the mean flow velocity, $U_{m(p=1)}$, can be estimated using the velocity–area method. As a consequence, $\phi(M_{com,p=1})$ can be computed using Equation (2), using $U_{m(p=1)}$ and $U_{max(p=1)}$. The iteration continues until the error of $\phi(M_{com,p}) - \phi(M)$ becomes lower than 0.01. For more details, the reader is referred to Moramarco et al. [46]. Table 2 summarizes the different flow conditions and their calculated entropic parameter magnitudes. Note that the discharge data in Table 1 were evaluated based on a statistical analysis of a sample of 30 years (1990–2020) of data. For the current data, the entropic parameter was decreased by increasing the flow discharge, depicting a decreasing trend. The magnitudes and the range of the entropic parameter agree with the data reported in previous works such as Bahmanpouri et al. [32] for large rivers and Chiu et al. [52], Choo et al. [53], Greco [54] and Moramarco [55], Moramarco et al. [56], Bahmanpouri et al. [34], and Bahmanpouri et al. [37] for small rivers.

Table 2. Different flow conditions and entropic parameter values.

Flow Condition	Mean Velocity (m/s)	Discharge (m^3/s)	$\phi(M)$	M
Low flow	0.8	355.4	0.8	4.8
Moderate flow	1.59	948	0.775	4.2
High flow	2.06	1587.9	0.763	3.9

2.3. Bed-Load Sediment Rate

The theoretical prediction of the critical threshold for the initiation of motion relies on establishing an equilibrium between the destabilizing hydrodynamic drag and lift forces and the resisting gravitational and frictional forces. In addition to factors like the slope of the bed, particle exposure, and pocket geometry, a precise estimation of the incipient motion necessitates a thorough understanding of the hydrodynamic drag and lift forces exerted on the particle [56–59]. Particle motion occurs when the fluid force acting on a particle is slightly greater than the resisting force associated with the weight of the submerged particle and the friction coefficient. Initial investigations into the onset of motion were carried out by Brahms [60], who proposed a relationship between the flow velocity and the necessary weight of a stone for stability, and by Dubuat [61], who introduced the concept of critical bed shear stress. By introducing Shields mobility parameter, the particle motion occurs if

$$\theta > \theta_{cr} \tag{5}$$

where θ is the Shields mobility parameter [62–64]:

$$\theta = \frac{u^{*2}}{(s-1)gd} = \frac{\tau_b}{(\rho_s - \rho)gd} \tag{6}$$

where u^* is the shear velocity, $s = \rho_s/\rho$ is the relative density, g is the acceleration of gravity, and τ_b is the bed shear stress. u^* under the assumption of normal flow and satisfying the Manning–Strickler resistance relationship can be written as [65]:

$$u^* = \sqrt{\frac{\tau_b}{\rho}} = \sqrt{ghs_f} \tag{7}$$

where s_f is the water-surface slope or friction slope and h is the vertical depth. S_f is calculated based on Manning's equation for each vertical according to the entropy velocity:

$$u_E = \frac{1}{n} R^{2/3} s_f^{1/2} \tag{8}$$

where u_E is the entropy output velocity and R is the hydraulic radius, which, for wide channels, is equal to h. n can be calculated based on the empirical correlation for the Gauckler–Manning coefficient of rivers [66]:

$$n = 0.041 d_{50}^{1/6} \tag{9}$$

A dimensionless Einstein bed-load rate $\overline{q}_b^*$ can be defined as follows [67]:

$$q_b^* = \frac{q_b}{D_m (RgD_m)^{0.5}} \tag{10}$$

where D_m is the arithmetic mean diameter of the sediment and R is the submerged specific gravity ($R = s - 1$). Meyer-Peter and Müller [4] (MPM) introduced the following bed-load relationship:

$$q_b^* = 8(\theta - \theta_{cr})^{1.5} \qquad \theta_{cr} = 0.047 \tag{11}$$

Wong and Parker [68] based on experimental data modified the bed-load relationship of Meyer-Peter and Müller as follows:

$$q_b^* = 3.97(\theta - \theta_{cr})^{1.5} \qquad \theta_{cr} = 0.0495 \tag{12}$$

3. Results and Discussions

The obtained values of $\phi(M)$ for the present study ($0.66 < \phi(M) < 0.80$) were in agreement with the data reported for small rivers (e.g., $0.66 < \phi(M) < 0.80$ for natural channels in the United States [52], $0.6 < \phi(M) < 0.68$ for the Tiber River in Italy [55], $0.63 < \phi(M) < 0.69$ for the Godavari and Ulhas Rivers in India [31] and for large rivers (e.g., $0.4 < \phi(M) < 0.61$ for the Amazon River in Brazil [32] and $0.60 < \phi(M) < 0.73$ for the Sajó and the Freiberger Mulde Rivers). Also, $\phi(M) = 0.88$ (Hii River data of Shinohara and Tsubaki [69]) and $\phi(M) = 0.91$ (Leo-River data of Leopold [70]) were reported by Choo et al. [53]. It should be noted that the limitation of the model is that it cannot be used for sites where it is impossible to measure the surface velocity measurements.

In the present study, the location with the maximum surface velocity corresponded to the transverse vertical, where the maximum velocity generally occurs, as demonstrated by Corato et al. [71], Guo and Julien [72], and Moramarco et al. [45]. The cross-sectional velocity distribution for three flow conditions (as mentioned in Table 1) is presented in Figures 2–4. The input data were bathymetry and single velocity data collected using a current meter for each flow condition. The distribution of the surface velocity in the entropy model was based on two scenarios of parabolic and elliptic surface-velocity distributions (see the Appendix B). According to Nezu et al. [73], in rivers with an aspect ratio (river width/flow depth) lower than the critical value of 5, a velocity dip is formed; however, in the present study, with aspect ratios of 30.3, 26.7, and 23.3 for the low-, moderate-, and high-flow conditions, respectively, no significant velocity dip was observed. A velocity dip, i.e., the formation of the maximum velocity below the water surface, is mainly induced by secondary flows [22,46]. A similar finding was reported by Bahmanpouri et al. [32,34] and Kundu and Goshal [74] for both large and small rivers in terms of discharge. In natural rivers, turbulence causes momentum mixing and sediment redistribution, significantly affecting sediment density and viscosity, which consequently changes the velocity profile [75–77]. Turbulent intensity increases due to the roughness and is further intensified by a higher Froude number in the channel [78,79].

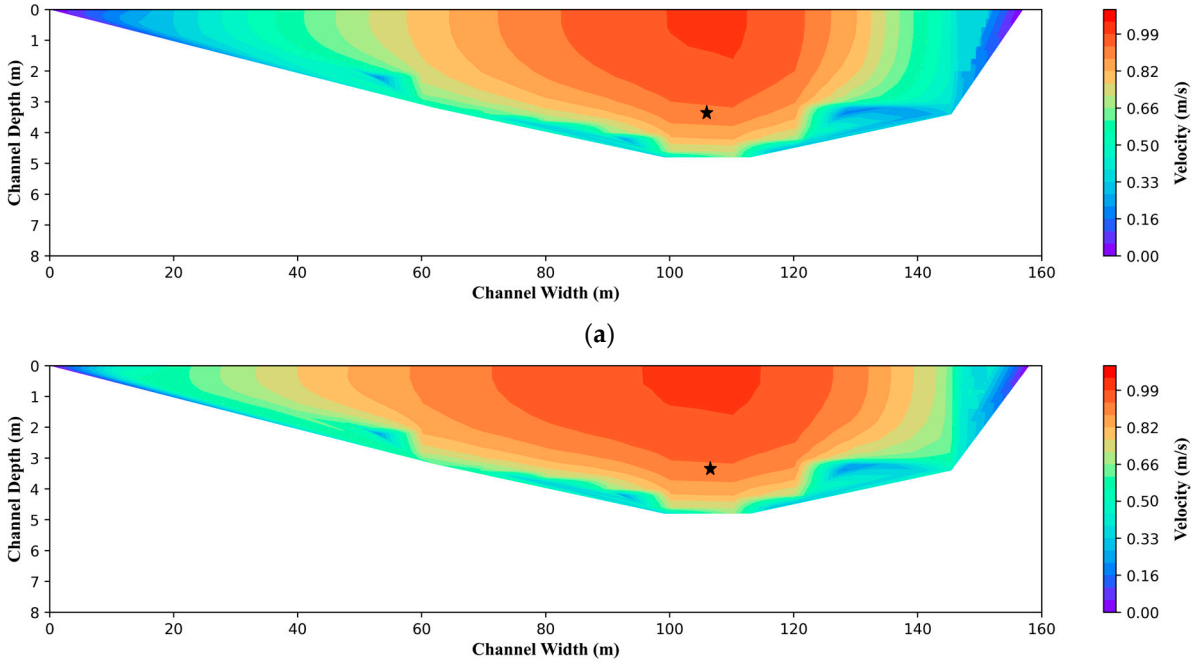


Figure 2. Cross-sectional distribution of velocity based on entropy model (low-flow condition). $U_{0.6D}$ is shown by a black star symbol. (**a**) Based on parabolic surface-velocity distribution; (**b**) based on elliptic surface-velocity distribution.

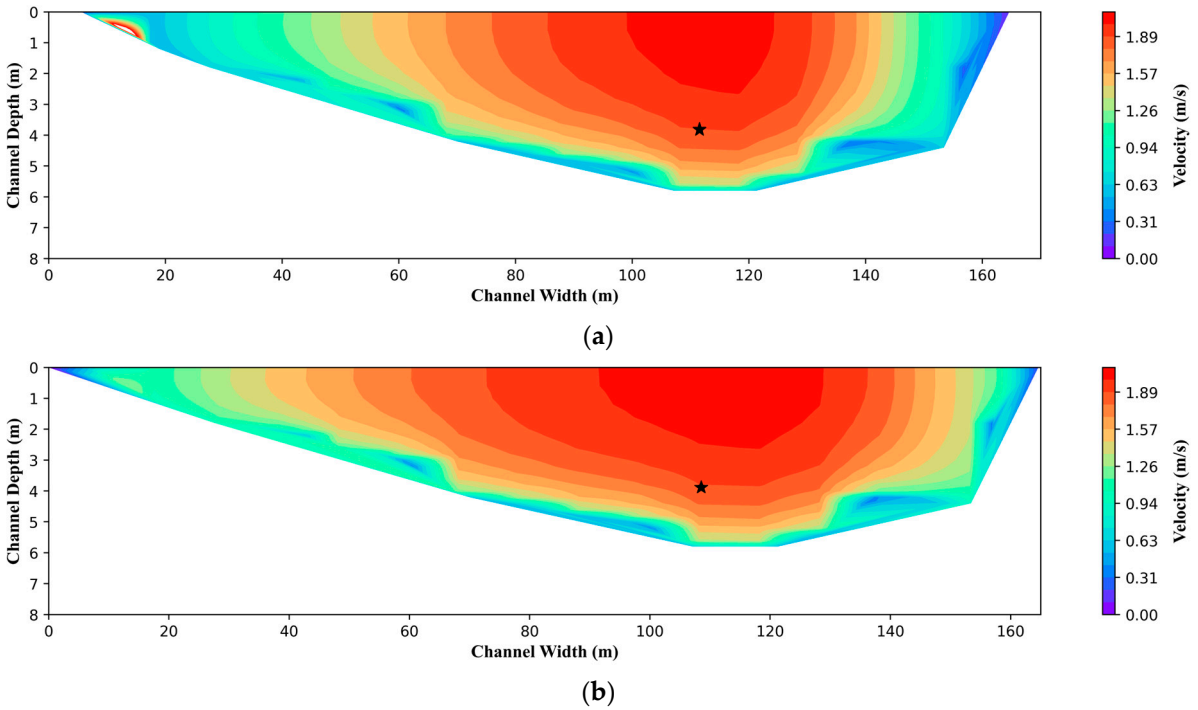


Figure 3. Cross-sectional distribution of velocity based on entropy model (moderate-flow condition). $U_{0.6D}$ is shown by a black star symbol. (**a**) Based on parabolic surface-velocity distribution; (**b**) based on elliptic surface-velocity distribution.

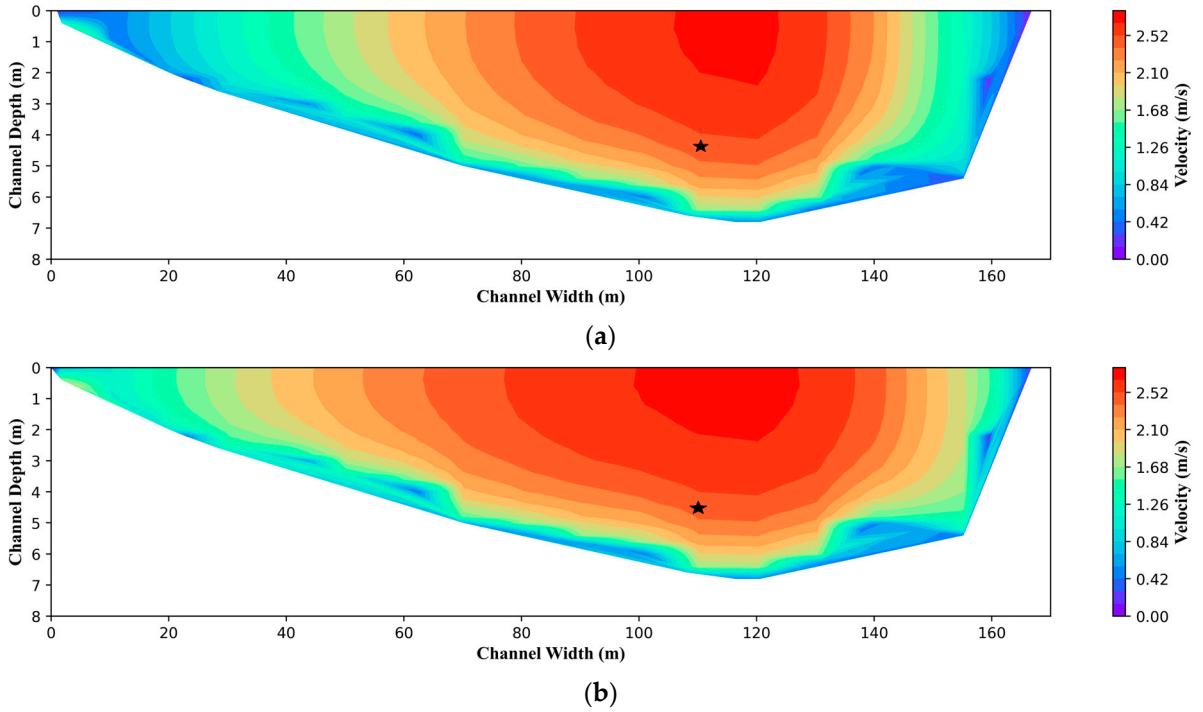


Figure 4. Cross-sectional distribution of velocity based on entropy model (high-flow condition). $U_{0.6D}$ is shown by a black star symbol. (**a**) Based on parabolic surface-velocity distribution; (**b**) based on elliptic surface-velocity distribution.

Table 3 presents the error percentage for estimating the discharge under the different flow conditions based on both parabolic and elliptic scenarios of surface velocity. The results based on the elliptic scenario were much more accurate than those based on the parabolic scenario (less than 2 and 9 percent, respectively) for all flow conditions. Overall, the error percentage based on both scenarios was lower than 9 percent.

Table 3. Error percentage for estimating the mean velocity and discharge.

Flow Condition	Surface Velocity Scenario	Discharge (m^3/s)		Error Percentage (%)
		Observed	Estimated	
Low flow	Parabolic	355.4	333.9	6.0
	Elliptic		362.2	2.0
Moderate flow	Parabolic	948	883.3	6.8
	Elliptic		965.2	1.8
High flow	Parabolic	1587.9	1453.6	8.4
	Elliptic		1613.1	1.5

The shear-velocity results agreed with the findings of Neil [80], Afzalimehr and Anctil [81], and Afzalimehr and Rennie [82] on gravel beds and the data of Blanckaert et al. [83] for fine sediments in laboratory experiments. Researchers have conducted different field studies [84–87] and experimental investigations [88–92] on sediment transport and mentioned different ranges for bed roughness. Therefore, since d_{50} is an uncertain parameter, in the present study, a range for d_{50} was chosen based on previous literature on the dimension of the particles.

The results of the Shields mobility parameter follow the Shields diagram developed in previous studies, such as Parker [63]. According to Cheng et al. [93], zero-rate transport can

only happen when the bed shear stress approaches the threshold for motion, depending on the selected transport formula. Additionally, researchers such as Buffington [94] and Shih and Diplas [95] proposed that when extending bed-load data to the actual zero rate, the critical shear stress obtained should consistently tend toward zero.

Figure 5 depicts the dimensionless bed-load transport rate based on Meyer-Peter and Müller [4] for all flow conditions. The results agree with the Shields diagram, e.g., the one developed by Parker [63]. That is, by increasing the particle diameter or the relevant Reynolds number, the sediment load rate decreases (Figure 5). The inclusion of a correction for form drag is a notable feature of the Meyer-Peter and Müller [4] bed-load equation. This correction takes into account the flow resistance of the stream bed and considers factors beyond just skin friction, such as bed forms or the movement of bed-load particles. After conducting flume experiments, MPM discovered that a flow resistance relationship based solely on skin friction, utilizing Strickler [66]'s and Nikuradse [96]'s theories, resulted in an underestimation of the overall bed resistance.

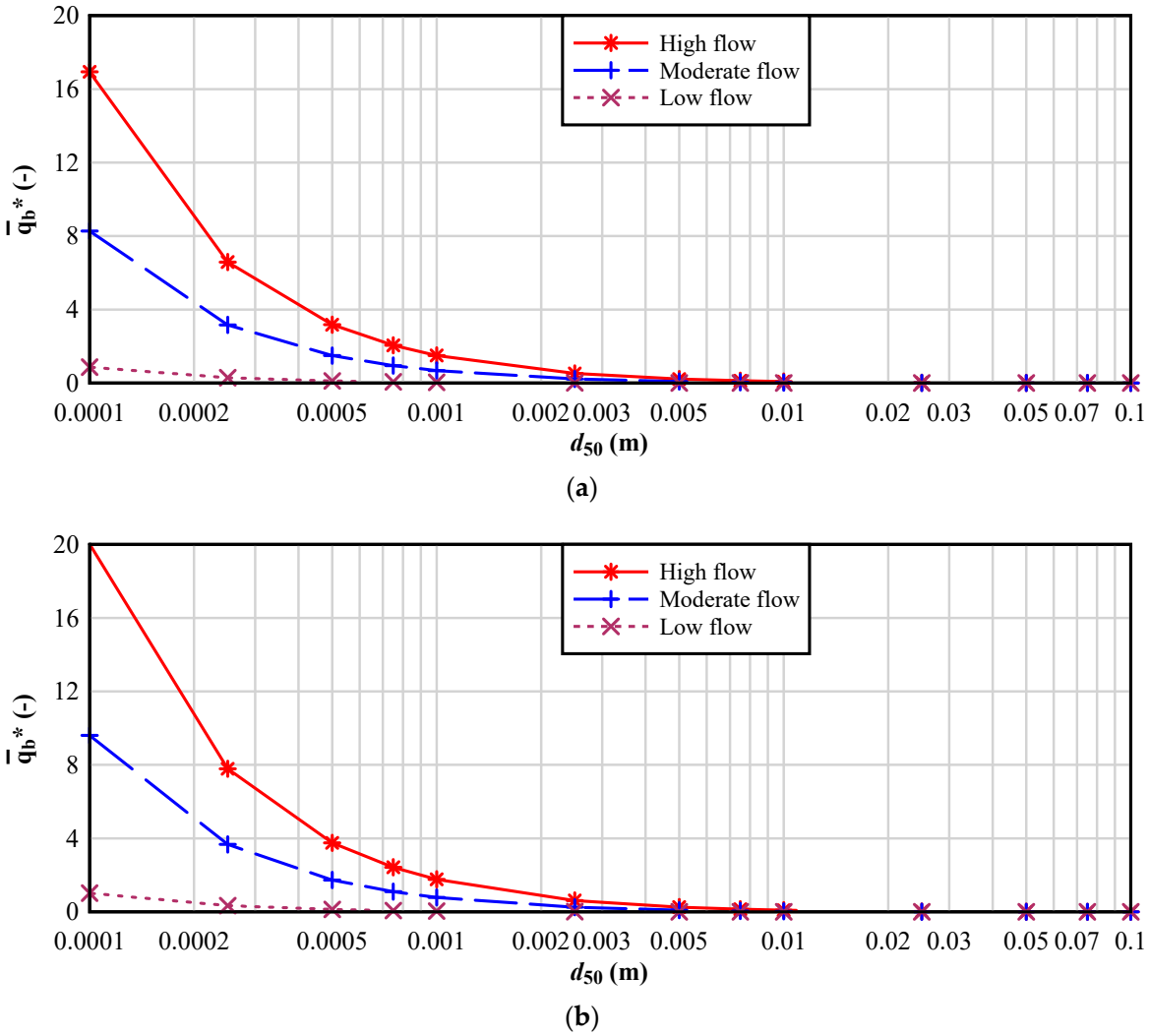


Figure 5. Distribution of the dimensionless bed-load transport rate (high-flow condition). (**a**) Parabolic scenario; (**b**) elliptic scenario.

Figure 6 compares the relationship between the Shields parameter and dimensionless sediment load with those from the literature. The present data were compared with the data of Parker [9] for two different particle dimeters of d_{50} = 5 and 28.5 mm; the experimental data of Meyer-Peter and Muller for two different particle sizes of d_{50} = 5.21 and 28.65 mm;

and the data of Gilbert for three different particle sizes of d_{50} = 3.17, 4.94, and 7.01 mm. It was noted that from the left bank to the right bank, each cross-section consisted of multiple verticals spaced at unique intervals, e.g., 1 m. For each vertical, the Shields mobility parameter was calculated for all cells from the bottom to the surface and then averaged across the entire cross-section. A bar notation was used to represent the average value of the parameter for the verticals.

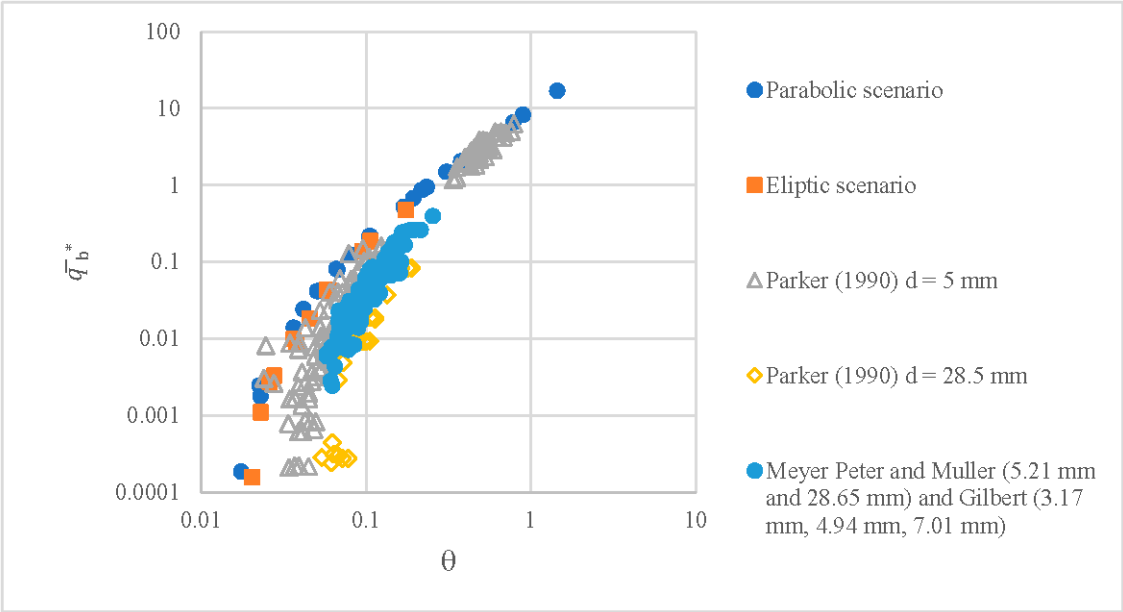
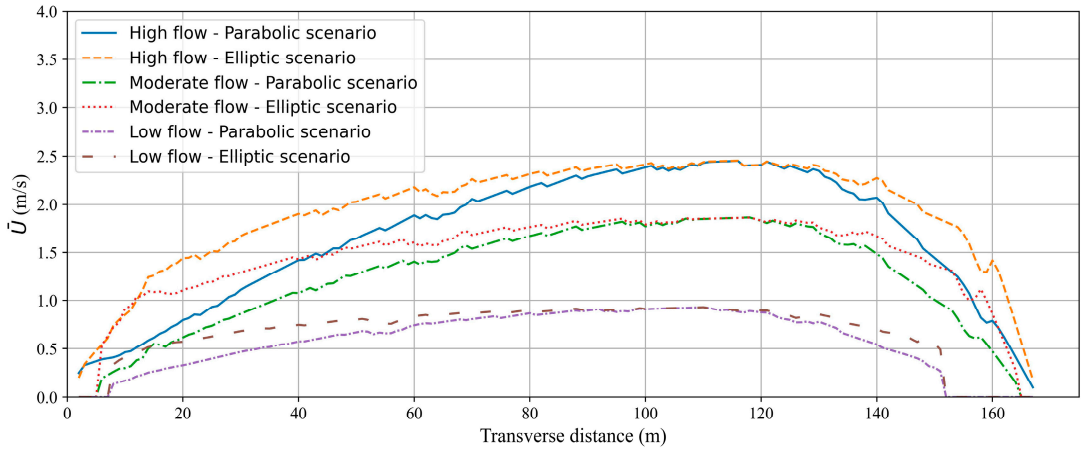


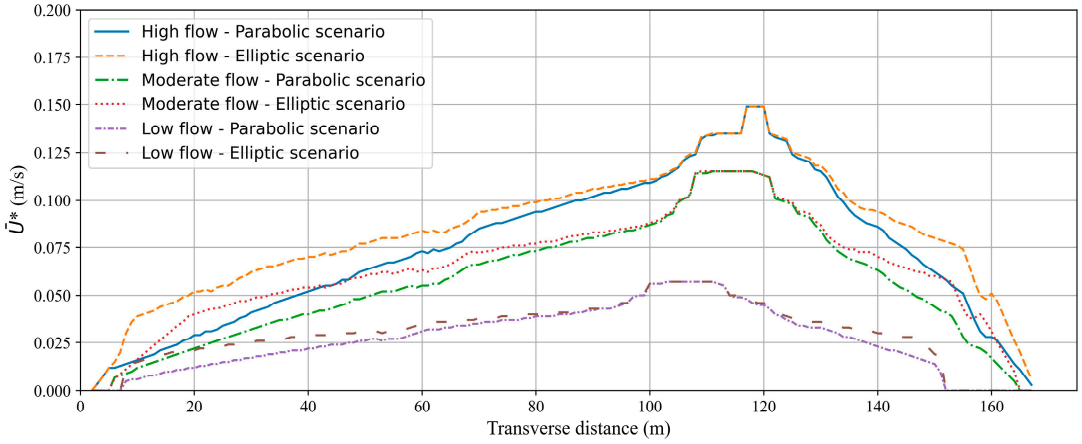
Figure 6. Relationship between Shields parameter and dimensionless bed-load transport rate.

Figure 7 presents the transverse distribution of the dimensionless bed-load transport rate, and mean and shear velocities for different flow conditions based on the grain size distribution in Figure 1c. As can be seen, the maximum bed-load transport was associated with large magnitudes of the mean and shear velocity for the different flow conditions with the assumption of uniform bed particles throughout the whole transverse length of the cross-section.

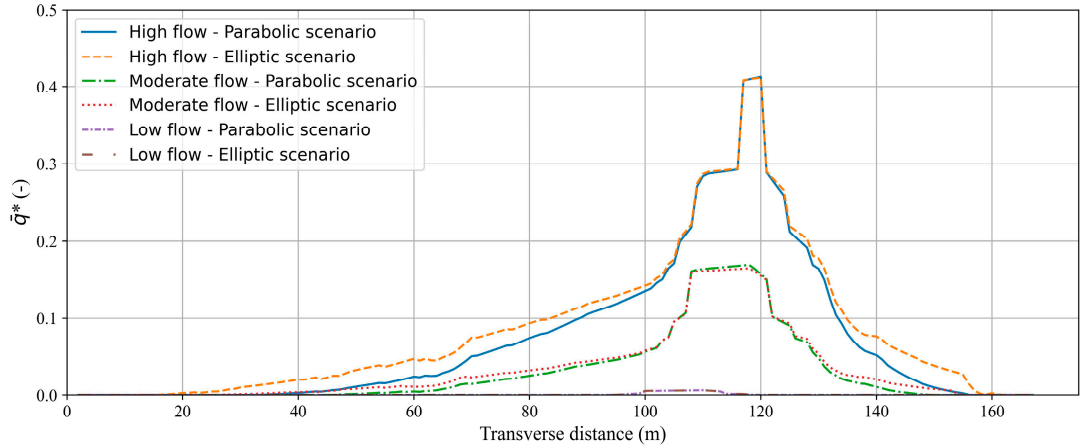


(**a**)

Figure 7. *Cont.*



(**b**)



(**c**)

Figure 7. Distribution of dimensionless bed-load transport rate and mean and shear velocities for different flow conditions. (**a**) Mean velocity; (**b**) shear velocity; (**c**) dimensionless bed-load transport.

4. Conclusions

The process of sediment transport was investigated in this study by employing the entropy concept as a theoretical procedure. Field data collected using a current meter in the Alaknanda River at Srinagar in India were employed. Two scenarios (parabolic and elliptic) for the distribution of the surface velocity were implemented in the entropy model. The estimated mean velocity and discharge values using the entropy model were compared with the observed data obtained from the Central Water Commission (CWC), highlighting a maximum error percentage of 9%. Next, shear velocity was determined for various cross-sections under different flow scenarios. The Shields parameter was calculated based on the shear-velocity distribution to assess the transport potential of sediment particles. The dimensionless bed-load transport obtained by the entropy model was in agreement with the available experimental data. A larger bed-load transport was observed at transverse locations with higher shear-velocity rates. The results depicted different rates of bed-load transport that increased with an increasing discharge rate and decreasing particle size. Overall, the study findings highlighted the potential of the entropy model as a theoretical approach for estimating river flow and sediment transport in developing countries where measurements of field velocities are often limited.

Author Contributions: Conceptualization, F.B., L.F. and T.M.; methodology, F.B. and T.M.; formal analysis and investigation, F.B., S.S., L.F. and T.M.; formal analysis, F.B., A.Y., C.M., D.D.S., A.S., A.A., S.S., L.F., T.M. and S.B.; writing—original draft preparation, F.B.; writing—review and editing, A.Y., C.M., D.D.S., A.S., A.A., S.S., L.F., T.M. and S.B.; funding acquisition, S.B. and S.S.; resources, S.B. and S.S.; supervision, S.B. All authors have read and agreed to the published version of the manuscript.

Funding: This work was supported by the 'Italy-India Joint Science and Technology Cooperation program for Joint Projects for the years 2021–2023' within the project FLOSET 'Probabilistic Floods and Sediment Transport Forecasting in the Himalayas During Extreme Events', funded by the Italian Ministry of Foreign Affairs and International Cooperation.

Data Availability Statement: Data will be made available on request.

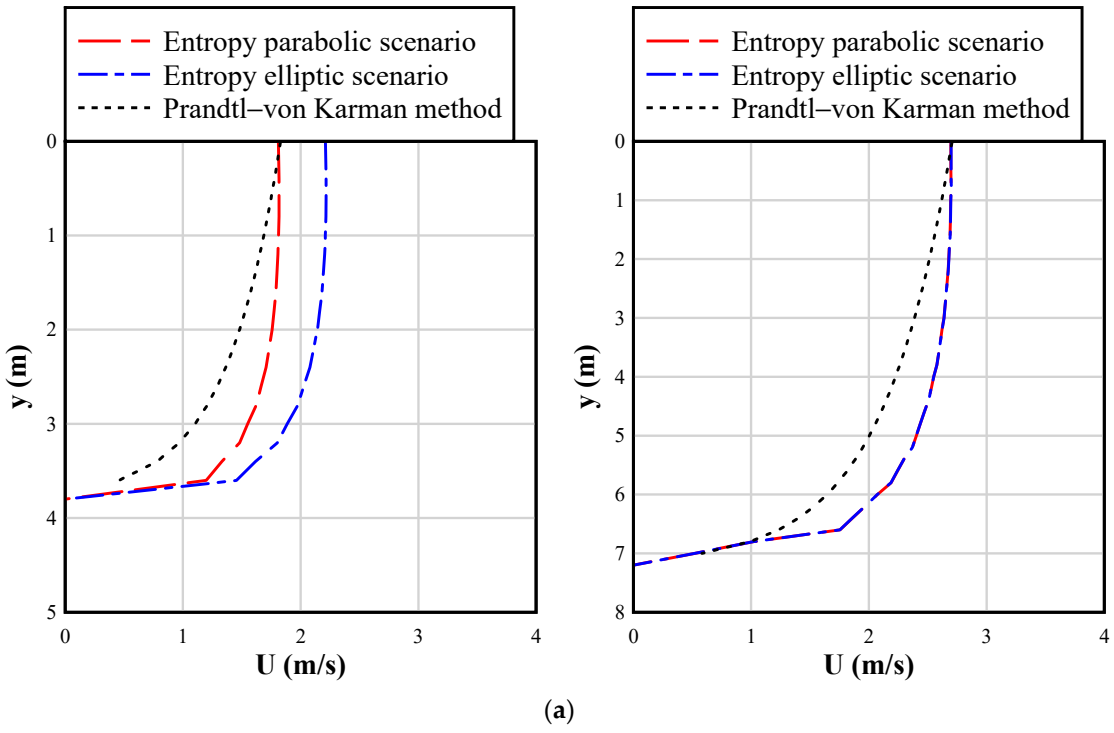
Conflicts of Interest: The authors have no competing interests to declare that are relevant to the content of this article.

Appendix A. Vertical Velocity Distribution

The Prandtl–von Karman universal velocity distribution law is the most common relationship for the vertical velocity distribution in channels [41]:

$$U = \frac{U^*}{k} \ln\left(\frac{y}{y_0}\right) \quad \text{(A1)}$$

where k is the von Karman constant (approximately 0.41) and y_0 is the value of y at which the velocity becomes zero. The vertical velocity at the transverse locations of 0.3 W and 0.7 W (W is the channel width) was compared with the Prandtl–von Karman velocity distribution for different flow conditions. Based on the Prandtl–von Karman velocity distribution, the maximum velocity was assumed to occur at the flow surface, while in the entropy model, it can be observed below the water surface as it considers the velocity dips induced by the existence of secondary currents.



(**a**)

Figure A1. *Cont.*

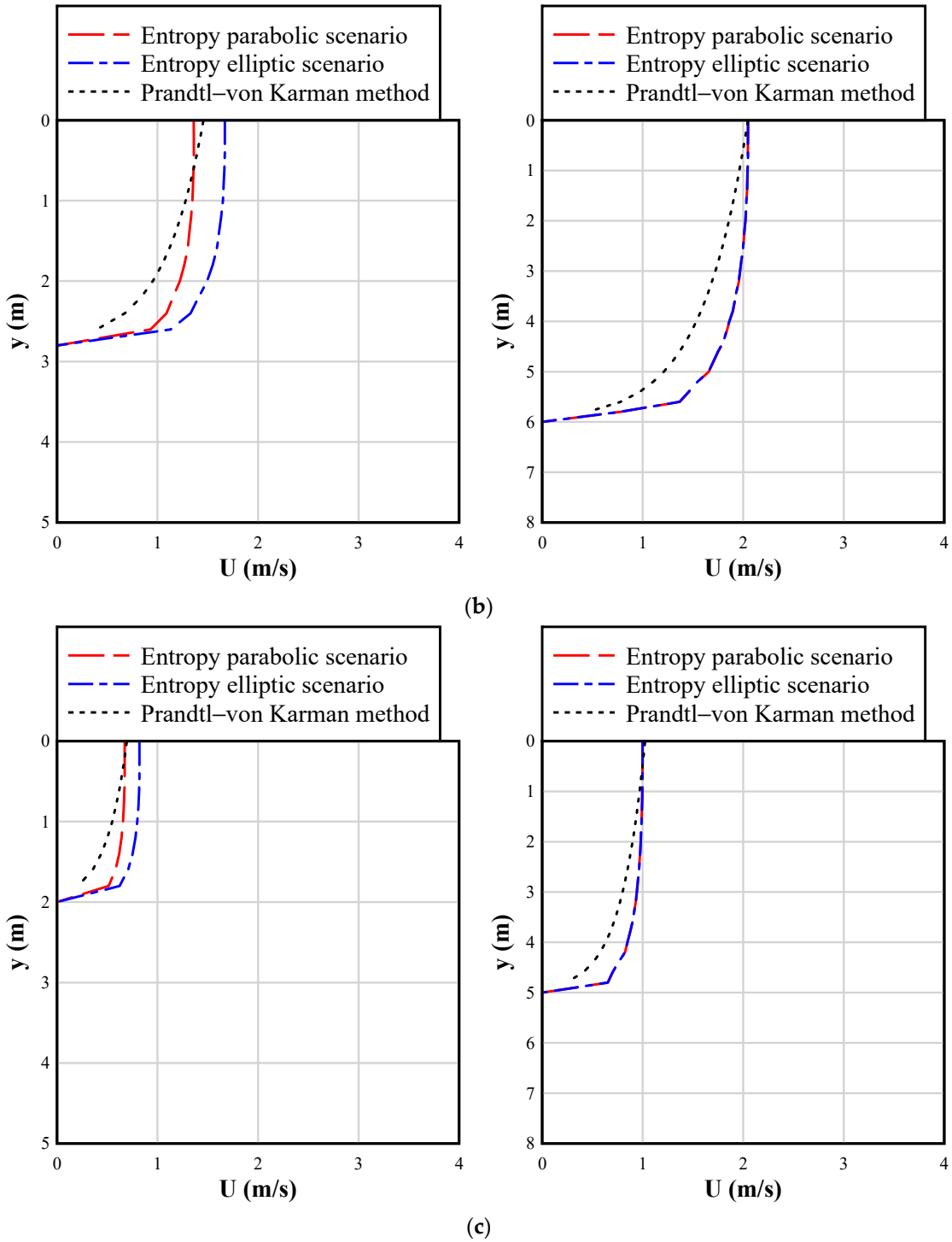


Figure A1. Vertical velocity distribution at two transverse locations of 0.3 W (**left**) and 0.7 W (**right**) for each flow condition. (**a**) High-flow condition; (**b**) moderate-flow condition; (**c**) low-flow condition.

Appendix B. Parabolic and Elliptic Surface Velocity Distributions

The mathematical relationships for the parabolic and elliptic surface-velocity distributions are shown below.

Parabolic:

$$U_{surf(i)} = U_{(\max_surf)} \times \left(1 - \frac{(x_{Umax_surf} - x_i)}{(x_{Umax_surf} - x_1)^2}\right) \qquad x(i) < x_{Umax_surf} \qquad \text{(A2)}$$

$$U_{surf(i)} = U_{(\max_surf)} \times (1 - \frac{(x_{Umax_surf} - x_i)}{(x_{last} - x_{Umax_surf})^2}) \qquad x(i) > x_{Umax_surf} \tag{A3}$$

Elliptic:

$$U_{surf(i)} = U_{(\max_surf)} \times (1 - \frac{(x_i - x_{Umax_surf})}{(x_{Umax_surf} - x_1)^2}) \qquad x(i) < x_{Umax_surf} \tag{A4}$$

$$U_{surf(i)} = U_{(\max_surf} \times (1 - \frac{(x_i - x_{Umax_surf})}{(x_{last} - x_{Umax_surf})^2}) \qquad x(i) > x_{Umax_surf} \tag{A5}$$

where $U_{surf(i)}$ is the surface velocity at the transverse vertical of i, $U_{(\max_surf)}$ is the maximum surface velocity, x_{Umax_surf} is the transverse location of the maximum surface velocity, and x_i is the transverse location of the vertical i.

References

1. Liu, Y.; Métivier, F.; Lajeunesse, É.; Lancien, P.; Narteau, C.; Ye, B.; Meunier, P. Measuring bed load in gravel bed mountain rivers: Averaging methods and sampling strategies. *Geodin. Acta* **2008**, *21*, 81–92. [CrossRef]
2. Yalin, M.S. *Mechanics of Sediment Transport*, 2nd ed.; Pergamon Press: Sydney, Australia, 1977.
3. Einstein, H.A. Formulas for the transportation of bed load. *Trans. Am. Soc. Civ. Eng.* **1942**, *107*, 561–597. [CrossRef]
4. Meyer-Peter, E.; Müller, R. Formulas for bed-load transport. In Proceedings of the 2nd Congress International Association for Hydraulic Research, Rotterdam, The Netherlands, 7–9 June 1948; pp. 39–64.
5. Bagnold, R.A. *An Approach to the Sediment Transport Problem from General Physics*; Geological Survey Professional Paper No. 422-I; U.S. Government Printing Office: Washington, DC, USA, 1966.
6. Engelund, F.; Hansen, E. *A Monograph on Sediment Transport in Alluvial Streams*; Teknisk Forlag: Copenhagen, Denmark, 1972.
7. Ackers, P.; White, W.R. Sediment transport: New approach and analysis. *J. Hydraul. Div.* **1973**, *99*, 2041–2060. [CrossRef]
8. Van Rijn, L.C. Sediment transport, part I: Bed load transport. *J. Hydraul. Eng.* **1984**, *110*, 1431–1456. [CrossRef]
9. Parker, G. Surface based bedload transport relation for gravel rivers. *J. Hydraul. Res.* **1990**, *28*, 417–436. [CrossRef]
10. Moramarco, T.; Saltalippi, C.; Singh, V.P. Velocity profiles assessment in natural channels during high floods. *Hydrol. Res.* **2011**, *42*, 162–170. [CrossRef]
11. Bonakdari, H.; Larrarte, F.; Lassabatere, L.; Joannis, C. Turbulent velocity profile in fully-developed open channel flows. *Environ. Fluid Mech.* **2008**, *8*, 1–17. [CrossRef]
12. Parker, G.; An, C.; Lamb, M.P.; Garcia, M.H.; Dingle, E.H.; Venditti, J.G. Dimensionless argument: A narrow grain size range near 2 mm plays a special role in river sediment transport and morphodynamics. *EGUsphere* **2023**, *2023*, 1–19. [CrossRef]
13. Yang, C.T.; Huang, C. Applicability of sediment transport formulas. *Int. J. Sediment Res.* **2001**, *16*, 335–353.
14. Gomez, B.; Church, M. An assessment of bed load sediment transport formulae for gravel bed rivers. *Water Resour. Res.* **1989**, *25*, 1161–1186. [CrossRef]
15. Barry, J.J.; Buffington, J.M.; King, J.G. A general power equation for predicting bed load transport rates in gravel bed rivers. *Water Resour. Res.* **2004**, *40*, W10401. [CrossRef]
16. Charru, F. Selection of the ripple length on a granular bed sheared by a liquid flow. *Phys. Fluids* **2006**, *18*, 121508. [CrossRef]
17. Charru, F.; Hinch, E. Ripple formation on a particle bed sheared by a viscous liquid. Part 1. Steady flow. *J. Fluid Mech.* **2006**, *550*, 111–121. [CrossRef]
18. Lajeunesse, E.; Malverti, L.; Charru, F. Bed load transport in turbulent flow at the grain scale: Experiments and modeling. *J. Geophys. Res. Earth Surf.* **2010**, *115*, F04001. [CrossRef]
19. Bonakdari, H.; Sheikh, Z.; Tooshmalani, M. Comparison between Shannon and Tsallis entropies for prediction of shear stress distribution in open channels. *Stoch. Environ. Res. Risk Assess.* **2015**, *29*, 1–11. [CrossRef]
20. Chiu, C.L. Velocity Distribution in Open Channel Flow. *J. Hydraul. Eng.* **1989**, *115*, 576–594. [CrossRef]
21. Chiu, C.L.; Said, C.A.A. Maximum and Mean Velocities and Entropy in Open-Channel Flow. *J. Hydraul. Eng.* **1995**, *121*, 26–35. [CrossRef]
22. Chiu, C.L.; Hsu, S.M.; Tung, N.C. Efficient methods of discharge measurements in rivers and streams based on the probability concept. *Hydrol. Process.* **2005**, *19*, 3935–3946. [CrossRef]
23. Ebtehaj, I.; Bonakdari, H.; Moradi, F.; Gharabaghi, B.; Khozani, Z.S. An integrated framework of Extreme Learning Machines for predicting scour at pile groups in clear water condition. *Coast. Eng.* **2018**, *135*, 1–15. [CrossRef]
24. Moramarco, T.; Singh, V.P. Formulation of the Entropy Parameter Based on Hydraulic and Geometric Characteristics of River Cross Sections. *J. Hydrol. Eng.* **2010**, *15*, 852–858. [CrossRef]
25. Singh, V.P.; Sivakumar, B.; Cui, H. Tsallis Entropy Theory for Modeling in Water Engineering: A Review. *Entropy* **2017**, *19*, 641. [CrossRef]
26. Sterling, M.; Knight, D. An attempt at using the entropy approach to predict the transverse distribution of boundary shear stress in open channel flow. *Stoch. Environ. Res. Risk Assess.* **2002**, *16*, 127–142. [CrossRef]

27. Termini, D.; Moramarco, T. Application of entropic approach to estimate the mean flow velocity and Manning roughness coefficient in a high-curvature flume. *Hydrol. Res.* **2017**, *48*, 634–645. [CrossRef]
28. Termini, D.; Moramarco, T. Entropic model application to identify cross-sectional flow effect on velocity distribution in a large amplitude meandering channel. *Adv. Water Resour.* **2020**, *143*, 103678. [CrossRef]
29. Abdolvandi, A.F.; Ziaei, A.N.; Moramarco, T.; Singh, V.P. New approach to computing mean velocity and discharge. *Hydrol. Sci. J.* **2021**, *66*, 347–353. [CrossRef]
30. Chahrour, N.; Castaings, W.; Barthélemy, E. Image-based river discharge estimation by merging heterogeneous data with information entropy theory. *Flow Meas. Instrum.* **2021**, *81*, 102039. [CrossRef]
31. Vyas, J.K.; Perumal, M.; Moramarco, T. Entropy based river discharge estimation using one-point velocity measurement at 0.6 D. *Water Resour. Res.* **2021**, *57*, e2021WR029825. [CrossRef]
32. Bahmanpouri, F.; Barbetta, S.; Gualtieri, C.; Ianniruberto, M.; Filizola, N.; Termini, D.; Moramarco, T. Prediction of river discharges at confluences based on Entropy theory and surface-velocity measurements. *J. Hydrol.* **2022**, *606*, 127404. [CrossRef]
33. Ammari, A.; Bahmanpouri, F.; Khelfi, M.E.A.; Moramarco, T. The regionalizing of the entropy parameter over the north Algerian watersheds: A discharge measurement approach for ungauged river sites. *Hydrol. Sci. J.* **2022**, *67*, 1640–1655. [CrossRef]
34. Bahmanpouri, F.; Eltner, A.; Barbetta, S.; Bertalan, L.; Moramarco, T. Estimating the Average River Cross-Section Velocity by Observing Only One Surface Velocity Value and Calibrating the Entropic Parameter. *Water Resour. Res.* **2022**, *58*, e2021WR031821. [CrossRef]
35. Ahamed, N.; Kundu, S. Fractional entropy-based modeling of suspended concentration distribution of type I and type II and sediment discharge in pipe and open-channel turbulent flows. *Z. Angew. Math. Phys.* **2023**, *74*, 101. [CrossRef]
36. Patel, P.; Sarkar, A. Entropic velocity distribution for sediment-laden flows with a modified dip estimation model at data-scarce river sites. *Hydrol. Sci. J.* **2024**, *69*, 746–764. [CrossRef]
37. Bahmanpouri, F.; Lazzarin, T.; Barbetta, S.; Moramarco, T.; Viero, D.P. Estimating flood discharge at river bridges using the entropy theory. Insights from Computational Fluid Dynamics flow fields. *Hydrol. Earth Syst. Sci.* **2024**, *28*, 3717–3737. [CrossRef]
38. Singh, S.; Kansal, M.L. Sub-basin prioritisation using RUSLE in a Mountainous River Basin of Uttarakhand (India). *Environ. Dev. Sustain.* **2024**, *26*, 6851–6877. [CrossRef]
39. Church, M.A. River bed gravels: Sampling and analysis. In *Sediment Transport in Gravel-Bed Rivers*; Wiley: Hoboken, NJ, USA, 1987; pp. 43–88.
40. Yadav, A.; Sen, S.; Mao, L.; Hassan, M.A. Estimation of bed material transport in gravel-bed streams using the virtual velocity approach: Insights from the North-Western Himalayas, India. *Earth Surf. Process. Landf.* **2024**, *49*, 3367–3382. [CrossRef]
41. Chiu, C.L. Entropy and probability concepts in hydraulics. *J. Hydraul. Eng.* **1987**, *113*, 583–599. [CrossRef]
42. Chiu, C.L. Entropy and 2-D velocity distribution in open channels. *J. Hydraul. Eng.* **1988**, *114*, 738–756. [CrossRef]
43. Chiu, C.L. Application of entropy concept in open-channel flow study. *J. Hydraul. Eng.* **1991**, *117*, 615–628. [CrossRef]
44. Chin, C.L.; Murray, D.W. Variation of velocity distribution along nonuniform open-channel flow. *J. Hydraul. Eng.* **1992**, *118*, 989–1001. [CrossRef]
45. Moramarco, T.; Saltalippi, C.; Singh, V.P. Estimation of mean velocity in natural channels based on Chiu's velocity distribution equation. *J. Hydrol. Eng.* **2004**, *9*, 42–50. [CrossRef]
46. Moramarco, T.; Barbetta, S.; Tarpanelli, A. From surface flow velocity measurements to discharge assessment by the entropy theory. *Water* **2017**, *9*, 120. [CrossRef]
47. Fulton, J.; Ostrowski, J. Measuring real-time streamflow using emerging technologies: Radar, hydroacoustics, and the probability concept. *J. Hydrol.* **2008**, *357*, 1–10. [CrossRef]
48. Yang, S.Q.; Tan, S.K.; Lim, S.Y. Velocity distribution and dip-phenomenon in smooth uniform open channel flows. *J. Hydraul. Eng.* **2004**, *130*, 1179–1186. [CrossRef]
49. Piton, G.; Recking, A.; Le Coz, J.; Bellot, H.; Hauet, A.; Jodeau, M. Reconstructing depth-averaged open-channel flows using image velocimetry and photogrammetry. *Water Resour. Res.* **2018**, *54*, 4164–4179. [CrossRef]
50. Le Coz, J.; Hauet, A.; Pierrefeu, G.; Dramais, G.; Camenen, B. Performance of image-based velocimetry (LSPIV) applied to flash-flood discharge measurements in Mediterranean rivers. *J. Hydrol.* **2010**, *394*, 42–52. [CrossRef]
51. Muste, M.; Fujita, I.; Hauet, A. Large-scale particle image velocimetry for measurements in riverine environments. *Water Resour. Res.* **2008**, *44*, W00D19. [CrossRef]
52. Chiu, C.L.; Jin, W.; Chen, Y.C. Mathematical models of distribution of sediment concentration. *J. Hydraul. Eng.* **2000**, *126*, 16–23. [CrossRef]
53. Choo, T.H.; Jeong, I.J.; Chae, S.K.; Yoon, H.C.; Son, H.S. A study on deriving a mean velocity formula from Chiu's velocity formula and bottom shear stress. *Hydrol. Earth Syst. Sci.* **2011**, *8*, 6419–6442.
54. Greco, M.; Moramarco, T. Influence of bed roughness and cross section geometry on medium and maximum velocity ratio in open-channel flow. *J. Hydraul. Eng.* **2016**, *142*, 06015015. [CrossRef]
55. Moramarco, T.; Barbetta, S.; Bjerklie, D.M.; Fulton, J.W.; Tarpanelli, A. River bathymetry estimate and discharge assessment from remote sensing. *Water Resour. Res.* **2019**, *55*, 6692–6711. [CrossRef]
56. Lee, H.; Balachandar, S. Critical shear stress for incipient motion of a particle on a rough bed. *J. Geophys. Res. Earth Surf.* **2012**, *117*, F01026. [CrossRef]

57. Bahmanpouri, F.; Daliri, M.; Khoshkonesh, A.; Namin, M.M.; Buccino, M. Bed compaction effect on dam break flow over erodible bed; experimental and numerical modeling. *J. Hydrol.* **2021**, *594*, 125645. [CrossRef]
58. Mohanta, A.; Pradhan, A.; Mallick, M.; Patra, K.C. Assessment of shear stress distribution in meandering compound channels with differential roughness through various artificial intelligence approach. *Water Resour. Manag.* **2021**, *35*, 4535–4559. [CrossRef]
59. Khazaei Moughani, S.; Rezazadeh, S.; Azimmohseni, M.; Rahi, G.; Bahmanpouri, F. Applying a transfer function model to improve the sediment rating curve. *Int. J. River Basin Manag.* **2024**, 1–13. [CrossRef]
60. Brahms, A. *Anfangsgründe der Deich-und Wasser-Baukunst*; Tapper: Aurich, Germany, 1754; Volume 2.
61. DuBuat, P. *Principes d'Hydraulique*; L'Imprimerie de Monsieur: Paris, France, 1786.
62. White, S.J. Plane Bed Thresholds of fine Grained Sediments. *Nature* **1970**, *228*, 152–153. [CrossRef] [PubMed]
63. Parker, G. 1D Sediment Transport Morphodynamics with Applications to Rivers and Turbidity Currents. E-book Available at Gary Parker's Morphodynamics Web Page, Last Update 13 April 2006. 2004. Available online: http://hydrolab.illinois.edu/people/parkerg/ (accessed on 3 December 2024).
64. Safari, M.J.S.; Ebtehaj, I.; Bonakdari, H.; Es-haghi, M.S. Sediment transport modeling in rigid boundary open channels using generalize structure of group method of data handling. *J. Hydrol.* **2019**, *577*, 123951. [CrossRef]
65. Henderson, F.M. *Open Channel Flow*; MacMillan Company: New York, NY, USA, 1966.
66. Strickler, A. *Beiträge zur Frage der Geschwindigkeitsformel und der Rauhligkeitszahlen für Ströme, Kanäle und Geschlossene Leitungen. (Contributions to the Question of a Velocity Formula and Roughness Data for Streams, Channels and Closed Pipelines)*; Translation T-10, W.M. Keck Laboratory of Hydraulics and Water Resources, California Institute of Technology, USA, 1981; Mitt. des Eidgenössischen Amtes für Wasserwirtschaft: Bern, Switzerland, 1923; Volume 16. (In German)
67. Einstein, H.A. *The Bed-Load Function for Sediment Transportation in Open Channel Flows*; Technical Bulletin 1026; United States of Agriculture, Soil Conservation Service: Washington, DC, USA, 1950.
68. Wong, M.; Parker, G. Reanalysis and correction of bed-load relation of Meyer-Peter and Müller using their own database. *J. Hydraul. Eng.* **2006**, *132*, 1159–1168. [CrossRef]
69. Shinohara, K.; Tsubaki, T. *On the Characteristics of Sand Waves Formed upon the Beds of the Open Channels and Rivers*; Research Institute for Applied Mechanics, Kyushu University: Fukuoka, Japan, 1959.
70. Leopold, L.B. River channel change with time: An example: Address as retiring president of the Geological Society of America, Minneapolis, Minnesota, November 1972. *Geol. Soc. Am. Bull.* **1973**, *84*, 1845–1860. [CrossRef]
71. Corato, G.; Moramarco, T.; Tucciarelli, T. Discharge estimation combining flow routing and occasional measurements of velocity. *Hydrol. Earth Syst. Sci.* **2011**, *15*, 2979–2994. [CrossRef]
72. Guo, J.; Julien, P.Y. Application of modified log-wake law in open-channels. In *World Environmental and Water Resource Congress 2006: Examining the Confluence of Environmental and Water Concerns*; American Society of Civil Engineers: Reston, VA, USA, 2006; pp. 1–9.
73. Nezu, I.; Tominaga, A.; Nakagawa, H. Field measurements of secondary currents in straight rivers. *J. Hydraul. Eng.* **1993**, *119*, 598–614. [CrossRef]
74. Kundu, S.; Ghoshal, K. An Entropy Based Model for Velocity-Dip-Position. *J. Environ. Inform.* **2019**, *33*, 113–128. [CrossRef]
75. Bahmanpouri, F.; Termini, D.; Barbetta, S.; Gualtieri, C.; Dionigi, M.; Moramarco, T. Investigating hydrodynamics and turbulent effects in rivers for different flow conditions using spatial complexity metrics. *J. Hydrol.* **2024**, *641*, 131790. [CrossRef]
76. Cui, H.; Singh, V.P. Suspended sediment concentration in open channels using Tsallis entropy. *J. Hydrol. Eng.* **2014**, *19*, 966–977. [CrossRef]
77. Audisio, C.; Pasculli, A.; Sciarra, N. Conceptual and numerical models applied on the river pellice (North Western Italy). In *Engineering Geology for Society and Territory-Volume 3: River Basins, Reservoir Sedimentation and Water Resources*; Springer International Publishing: Cham, Switzerland, 2015; pp. 327–330.
78. Pasculli, A. Viscosity variability impact on 2D laminar and turbulent Poiseuille velocity profiles; Characteristic-Based Split (CBS) stabilization. In Proceedings of the 2018 5th International Conference on Mathematics and Computers in Sciences and Industry (MCSI), Corfu, Greece, 25–27 August 2018; IEEE: Piscataway, NJ, USA, 2018; pp. 128–134.
79. Bahmanpouri, F.; Gualtieri, C.; Chanson, H. Experiments on two-phase flow in hydraulic jump on pebbled rough bed: Part 1–Turbulence properties and particle chord time and length. *Water Sci. Eng.* **2023**, *16*, 359–368. [CrossRef]
80. Neill, C.R. *A Re-Examination of the Beginning of Movement for Coarse Granular Bed Materials*; Hydraulics Research Station: Wallingford, UK, 1968; p. 37.
81. Afzalimehr, H.; Anctil, F. Velocity distribution and shear velocity behaviour of decelerating flows over a gravel bed. *Can. J. Civ. Eng.* **1999**, *26*, 468–475. [CrossRef]
82. Afzalimehr, H.; Rennie, C.D. Determination of bed shear stress in gravel-bed rivers using boundary-layer parameters. *Hydrol. Sci. J.* **2009**, *54*, 147–159. [CrossRef]
83. Blanckaert, K.; Heyman, J.; Rennie, C.D. Measuring bedload sediment transport with an acoustic doppler velocity profiler. *J. Hydraul. Eng.* **2017**, *143*, 04017008. [CrossRef]
84. Fujita, I.; Muste, M.; Kruger, A. Large-scale particle image velocimetry for flow analysis in hydraulic engineering applications. *J. Hydraul. Res.* **1998**, *36*, 397–414. [CrossRef]
85. Church, M. *The Regulation of Peace River: A Case Study for River Management*; John Wiley & Sons: Hoboken, NJ, USA, 2014.

86. Lamb, M.P.; Venditti, J.G. The grain size gap and abrupt gravel-sand transitions in rivers due to suspension fallout. *Geophys. Res. Lett.* **2016**, *43*, 3777–3785. [CrossRef]
87. Dingle, E.H.; Kusack, K.M.; Venditti, J.G. The gravel-sand transition and grain size gap in river bed sediments. *Earth-Sci. Rev.* **2021**, *222*, 103838. [CrossRef]
88. Parker, G. Progress in the modeling of alluvial fans. *J. Hydraul. Res.* **1999**, *37*, 805–825. [CrossRef]
89. Wilcock, P.R.; Crowe, J.C. Surface-based transport model for mixed-size sediment. *J. Hydraul. Eng.* **2003**, *129*, 120–128. [CrossRef]
90. Ahadiyan, J.; Bahmanpouri, F.; Adeli, A.; Gualtieri, C.; Khoshkonesh, A. Riprap effect on hydraulic fracturing process of cohesive and non-cohesive protective levees. *Water Resour. Manag.* **2022**, *36*, 625–639. [CrossRef]
91. Dingle, E.H.; Venditti, J.G. Experiments on gravel-sand transitions: Behavior of the grain size gap material. *J. Geophys. Res. Earth Surf.* **2023**, *128*, e2023JF007117. [CrossRef]
92. Church, M.; Hassan, M.A. The fluvial grain size gap: Experimental confirmation of hydraulic origin. *Earth Surf. Process. Landf.* **2023**, *48*, 1502–1511. [CrossRef]
93. Cheng, N.S.; Lu, C.; Lu, Y.; Wei, M.; Zheng, L. Quantitative definition of Shields criterion for incipient sediment motion. *Int. J. Sediment Res.* **2024**, *39*, 61–69. [CrossRef]
94. Buffington, J.M. The legend of AF Shields. *J. Hydraul. Eng.* **1999**, *125*, 376–387. [CrossRef]
95. Shih, W.; Diplas, P. A unified approach to bed load transport description over a wide range of flow conditions via the use of conditional data treatment. *Water Resour. Res.* **2018**, *54*, 3490–3509. [CrossRef]
96. Nikuradse, J. *Laws of Flow in Rough Pipes*; National Advisory Committee for Aeronautics (NACA): Washington, DC, USA, 1950.

Disclaimer/Publisher's Note: The statements, opinions and data contained in all publications are solely those of the individual author(s) and contributor(s) and not of MDPI and/or the editor(s). MDPI and/or the editor(s) disclaim responsibility for any injury to people or property resulting from any ideas, methods, instructions or products referred to in the content.